



Evaluation of a  
chemistry transport  
model using a  
regional OMI NO<sub>2</sub>  
retrieval

G. Kuhlmann et al.

# Evaluation of a regional chemistry transport model using a newly developed regional OMI NO<sub>2</sub> retrieval

G. Kuhlmann<sup>1,\*</sup>, Y. F. Lam<sup>1</sup>, H. M. Cheung<sup>1</sup>, A. Hartl<sup>1</sup>, J. C. H. Fung<sup>2</sup>, P. W. Chan<sup>3</sup>,  
and M. O. Wenig<sup>4</sup>

<sup>1</sup>School of Energy and Environment, City University of Hong Kong, Hong Kong, China

<sup>2</sup>Department of Mathematics, The Hong Kong University of Science & Technology, Hong Kong, China

<sup>3</sup>Hong Kong Observatory, Hong Kong, China

<sup>4</sup>Meteorologisches Institut, Ludwig-Maximilians-Universität, Munich, Germany

\* now at: Empa, Swiss Federal Laboratories for Materials Science and Technology, Dübendorf, Switzerland

Received: 26 September 2014 – Accepted: 7 November 2014 – Published: 9 December 2014

Correspondence to: G. Kuhlmann (gerrit.kuhlmann@gmail.com) and  
Y. F. Lam (yunflam@cityu.edu.hk)

Published by Copernicus Publications on behalf of the European Geosciences Union.

Title Page

Abstract

Introduction

Conclusions

References

Tables

Figures

◀

▶

◀

▶

Back

Close

Full Screen / Esc

Printer-friendly Version

Interactive Discussion



## Abstract

In this paper, we evaluate a high-resolution chemistry transport model (CTM) (3 km × 3 km spatial resolution) with the new Hong Kong (HK) NO<sub>2</sub> retrieval developed for the Ozone Monitoring Instrument (OMI) on-board the Aura satellite. The three-dimensional atmospheric chemistry was modelled in the Pearl River Delta (PRD) region in southern China by the Models-3 Community Multiscale Air Quality (CMAQ) modelling system from October 2006 to January 2007. In the HK NO<sub>2</sub> retrieval, tropospheric air mass factors (AMF) were recalculated using high-resolution ancillary parameters of surface reflectance, NO<sub>2</sub> profile shapes and aerosol profiles of which the latter two were taken from the CMAQ simulation. We also tested four different aerosol parametrizations. Ground level measurements by the PRD Regional Air Quality Monitoring (RAQM) network were used as additional independent measurements.

The HK NO<sub>2</sub> retrieval increases the NO<sub>2</sub> vertical column densities (VCD) by (+31 ± 38) %, when compared to NASA's standard product (SP2), and reduces the mean bias (MB) between satellite and ground measurements by 26 percentage points from -41 to -15 %. The correlation coefficient  $r$  is low for both satellite datasets ( $r = 0.35$ ) due to the high spatial variability of NO<sub>2</sub> concentrations.

The correlation between CMAQ and the RAQM network is low ( $r \approx 0.3$ ) and the model underestimates the NO<sub>2</sub> concentrations in the north-western model domain (Foshan and Guangzhou). We compared the CMAQ NO<sub>2</sub> time series of the two main plumes with our regional OMI NO<sub>2</sub> product. The model overestimates the NO<sub>2</sub> VCDs by about 15 % in Hong Kong and Shenzhen, while the correlation coefficient is satisfactory ( $r = 0.56$ ). In Foshan and Guangzhou, the correlation is low ( $r = 0.37$ ) and the model underestimates the VCDs strongly (MB = -40 %). In addition, we estimated that the OMI VCDs are also underestimated by about 10 to 20 % in Foshan and Guangzhou because of the influence of the model parameters on the AMF.

In this study, we demonstrate that the HK OMI NO<sub>2</sub> retrieval reduces the bias of the satellite measurements and thus the dataset can be used to study the magnitude of

ACPD

14, 31039–31090, 2014

### Evaluation of a chemistry transport model using a regional OMI NO<sub>2</sub> retrieval

G. Kuhlmann et al.

Title Page

Abstract

Introduction

Conclusions

References

Tables

Figures

◀

▶

◀

▶

Back

Close

Full Screen / Esc

Printer-friendly Version

Interactive Discussion

## Evaluation of a chemistry transport model using a regional OMI NO<sub>2</sub> retrieval

G. Kuhlmann et al.

Title Page

Abstract

Introduction

Conclusions

References

Tables

Figures

◀

▶

◀

▶

Back

Close

Full Screen / Esc

Printer-friendly Version

Interactive Discussion



NO<sub>2</sub> concentrations in a regional model. The low bias can be achieved if AMFs are recalculated with more accurate surface reflectance, aerosol profiles and NO<sub>2</sub> profiles; only NO<sub>2</sub> profiles have been replaced in earlier studies. Since unbiased concentrations are important, for example, in air pollution studies, the results of this paper can be very helpful in future model evaluation studies.

## 1 Introduction

Nitrogen oxides (NO<sub>x</sub> = NO + NO<sub>2</sub>) play an important role in atmospheric chemistry. They have a vital role in the formation of photochemical smog (Haagen-Smit, 1952) and can damage crops and buildings as a component of acid rain (Driscoll et al., 2001). In an urban environment, NO<sub>2</sub> concentrations have a high spatial and temporal variability due to its short tropospheric life time and the variety of sources and sinks. The spatial and temporal distribution can be studied with chemistry transport models (CTM) and satellite instruments.

The first satellite instrument able to detect tropospheric NO<sub>2</sub> was the Global Ozone Monitoring Experiment (GOME) which was launched on board the second European Remote Sensing satellite (ERS-2) in 1995 (Burrows et al., 1999). Successor instruments to GOME (GOME-2) are payload on the MetOp satellites used for operational meteorology (Callies et al., 2000). In 2006, the Scanning Imaging Absorption Spectrometer for Atmospheric Cartography (SCIAMACHY) was launched on board ENVISAT (ENVIRONMENTAL SATellite) (Bovensmann et al., 1999) and in 2004, the Ozone Monitoring Instrument (OMI) was launched on board the EOS (Earth Observation System) Aura (Levelt et al., 2006). Since the launch of GOME, the spatial resolution of the instruments increased rapidly. While GOME had a smallest ground pixel size of 40 km × 320 km, OMI has a ground pixel size of 13 km × 24 km. The higher spatial resolution makes OMI feasible for the study of trace gases in large metropolitan areas.

The two OMI NO<sub>2</sub> standard products are the NASA standard product (SP) (Bucsela et al., 2006, 2013) and the the Dutch OMI NO<sub>2</sub> product (DOMINO) (Boersma et al.,

**Evaluation of a chemistry transport model using a regional OMI NO<sub>2</sub> retrieval**

G. Kuhlmann et al.

Title Page

Abstract

Introduction

Conclusions

References

Tables

Figures

◀

▶

◀

▶

Back

Close

Full Screen / Esc

Printer-friendly Version

Interactive Discussion

2007, 2011) which are both available in their second version (SP2 and DOMINO-2). In this paper, we use the term “global” products for this two products because they provide global coverage. In contrast, “regional” products provide regional coverage. Examples of regional OMI NO<sub>2</sub> products are the Empa product for Europe (Boersma et al., 2007; Zhou et al., 2009, 2010) and the Berkeley High-Resolution (BEHR) product for North America (Russell et al., 2011). It should be noted that in literature the term “global” is often used as a synonym for “level 3” data that has had orbit-level data (“level 2”) combined onto a global grid. This terminology can be misleading, because “level 3” data can also be provided on a local or regional grid. For example, the grid can be the domain of a regional CTM. A second difference between regional and global products is the spatiotemporal resolution of the ancillary parameters used in their retrieval algorithms. Ancillary parameters are information about surface reflectance, NO<sub>2</sub> profile shapes, aerosols and clouds which are used to calculate air mass factors (AMF) which convert the retrieved slant column densities (SCD) to vertical column densities (VCD). In the first version of SP and DOMINO, the ancillary parameters were mainly monthly or annual averages with spatial resolutions between 50 and 300 km. In contrast, regional products use ancillary parameters with a higher spatial and temporal resolution. For example, Zhou et al. (2010) used surface reflectance with 1 km spatial resolution to improve the NO<sub>2</sub> retrieval in Europe and Russell et al. (2011) replaced the profile shapes from a global CTM with profiles from a regional CTM with a spatial resolution of 4 km. Thus, we use the terms “regional” and “global” for products which use ancillary parameters which have a spatial and temporal resolution typical for a regional or global CTM, respectively.

Russell et al. (2011) compared the BEHR product with the first version of the DOMINO and the NASA product and showed that the retrieved NO<sub>2</sub> VCDs are strongly impacted by terrain pressure ( $\pm 20\%$ ), surface reflectance ( $\pm 40\%$ ) and the NO<sub>2</sub> profile shape ( $-75 \pm 10\%$ ). Lin et al. (2014) showed that different ancillary parameters can have a strong impact on the NO<sub>2</sub> VCDs. Furthermore, the global NO<sub>2</sub> products have been compared with regional CTMs. Since the OMI NO<sub>2</sub> VCDs depend on the NO<sub>2</sub>





within a ground pixel is nearly constant in across-track direction but decreases in along-track direction.

## 2.2 Retrieval of tropospheric NO<sub>2</sub> column densities

The standard product (SP2) (Bucsela et al., 2006, 2013) is the basis for the HK NO<sub>2</sub> retrieval. Therefore, we give a brief introduction to their algorithm. The SP2 retrieval algorithm has three major steps:

1. The total slant column densities  $S$  are obtained from the reflectance spectra using the differential optical absorption spectroscopy (DOAS) technique (Platt and Stutz, 2008).
2. The stratospheric slant column densities  $S_{\text{strat}}$  are subtracted from the total column  $S$  using a stratosphere–troposphere separation (STS) algorithm (Bucsela et al., 2013).
3. The tropospheric slant column densities  $S_{\text{trop}}$  are converted to vertical column density  $V_{\text{trop}}$  using a tropospheric air mass factors (AMF)  $A_{\text{trop}}$  (Palmer et al., 2001).

The AMF is defined as the ratio of slant and vertical column density (Solomon et al., 1987). Thus the tropospheric column density  $V_{\text{trop}}$  is calculated by

$$V_{\text{trop}} = \frac{S - S_{\text{strat}}}{A_{\text{trop}}} = \frac{S_{\text{trop}}}{A_{\text{trop}}}. \quad (1)$$

The tropospheric AMF depends on parameters such as sun position, satellite position, surface reflectance, atmospheric scattering properties due to air molecules, aerosols and clouds, and the NO<sub>2</sub> profile shape. It is related to the vertical sensitiv-

### Evaluation of a chemistry transport model using a regional OMI NO<sub>2</sub> retrieval

G. Kuhlmann et al.

Title Page

Abstract

Introduction

Conclusions

References

Tables

Figures

◀

▶

◀

▶

Back

Close

Full Screen / Esc

Printer-friendly Version

Interactive Discussion

ity of the satellite instrument and can be computed for  $N$  vertical layers by

$$A_{\text{trop}} = \frac{\sum_{k=1}^N \alpha_k m_k V_k}{\sum_{k=1}^N V_k} \quad (2)$$

with:

- $\alpha_k$ : an empirical temperature correction coefficient accounting for the temperature dependency of the  $\text{NO}_2$  absorption cross section,
- $m_k$ : the differential or box air mass factor which describes the instrument sensitivity for layer  $k$ ,
- $V_k$ : the partial  $\text{NO}_2$  VCD of layer  $k$ .

The correction coefficient  $\alpha_k$  can be computed by the empirical formula

$$\alpha_k = 1 - 0.003 \text{ K}^{-1} (T_k - T_{\text{ref}}) \quad (3)$$

where  $T_k$  is the temperature in layer  $k$  and  $T_{\text{ref}}$  is reference temperature of the  $\text{NO}_2$  absorption cross section ( $T_{\text{ref}} = 220 \text{ K}$ ) (Bucsela et al., 2013).

The box air mass factors  $m_k$  can be computed with a radiative transfer model. The SP2 algorithm uses the TOMRAD radiative transfer model (Dave, 1965). The AMF formulation used in SP2 is based on a AMF formulation by Palmer et al. (2001). In partly cloudy scenes, SP2 computes the box AMFs using the independent pixel approximation (IPA). The approximation calculates AMFs as weighted sums of a cloudy  $m_k^{\text{cloudy}}$  and a clear  $m_k^{\text{clear}}$  component:

$$m_k = w \cdot m_k^{\text{cloudy}} + (1 - w) \cdot m_k^{\text{clear}}, \quad (4)$$

where  $w$  is the aerosol/cloud radiance fraction (CRF), that is the fraction of measured radiation that results from clouds and aerosols (Acarreta et al., 2004).

Evaluation of a chemistry transport model using a regional OMI  $\text{NO}_2$  retrieval

G. Kuhlmann et al.

Title Page

Abstract

Introduction

Conclusions

References

Tables

Figures

◀

▶

◀

▶

Back

Close

Full Screen / Esc

Printer-friendly Version

Interactive Discussion





## Evaluation of a chemistry transport model using a regional OMI NO<sub>2</sub> retrieval

G. Kuhlmann et al.

Title Page

Abstract

Introduction

Conclusions

References

Tables

Figures

◀

▶

◀

▶

Back

Close

Full Screen / Esc

Printer-friendly Version

Interactive Discussion



The products  $\alpha_k m_k$  are called scattering weights. They can be used to recalculate the AMF with different profile shapes which could be taken from a regional CTM.

In SP2, the partial VCD  $V_k$  are taken from the Global Modeling Initiative (GMI) CTM (Duncan et al., 2007; Strahan et al., 2007) which combines stratospheric chemistry described by Douglass et al. (2004) and tropospheric O<sub>3</sub>-NO<sub>x</sub>-hydrocarbon chemistry from the GEOS-Chem model (Bey et al., 2001). It should be noted that only the relative shape of the profile  $n_k = V_k/V_{\text{trop}}$  is required for the AMF calculation.

Bucsela et al. (2013) estimated tropospheric NO<sub>2</sub> VCD uncertainties to be  $1 \times 10^{15} \text{ cm}^{-2}$  for clear skies and up to  $3 \times 10^{15} \text{ cm}^{-2}$  for large cloud radiance fractions. In polluted regions, the main uncertainties are in the DOAS fit (10 % relative error) and in the tropospheric AMFs (20–80 %).

### 2.3 SCIATRAN radiative transfer model

SCIATRAN is a one-dimensional RTM which can be used for the calculation of box AMFs (Rozanov et al., 2005). The model is designed as a forward model for the retrieval of atmospheric constituents from measurements of scattered light by satellite, ground or airborne instruments. The wavelength range goes from 175 to 2380 nm which includes the ultra violet, visible and near infra red part of the spectrum.

SCIATRAN solves the integro-differential radiative transfer equation using the discrete-ordinates method (DOM) in the plane-parallel or pseudo-spherical mode to calculate box AMF profiles. Box AMFs  $m_k$  are derived from weighting functions which describe the sensitivity of the reflectance spectrum  $R$  to a perturbation of a model parameter  $\Delta n$  in layer  $z_k$ . In SCIATRAN, weighting functions are computed by a quasi-analytic approach (Rozanov et al., 1998). If  $\Delta n$  is a perturbation of the NO<sub>2</sub> number density  $n_k$ , the box AMF  $m_k$  is the negative weighting function (Rozanov and Rozanov, 2010).

### 3 Methodology

In this section, we describe the RAQM network, the regional CTM run and the HK NO<sub>2</sub> retrieval. Our study period is from October 2006 to January 2007. This period was chosen because cloud fractions in the PRD region are lowest in this season and OMI measurements in later years are affected by a row anomaly which reduces the number of valid measurements. Details about the row anomaly can be found on <http://www.knmi.nl/omi/research/product/rowanomaly-background.php>.

#### 3.1 Ground network

##### 3.1.1 Meteorological observations

Meteorological observations were used for the evaluation of the simulated meteorological fields which were used to drive the CTM. The data were measured by three automatic weather stations in Hong Kong. The stations are at the Hong Kong Observatory (HKO) headquarters, at the Hong Kong International Airport (HKIA) near Tung Chung and on Waglan Island (WGL). The locations of the stations are shown by square markers in Fig. 1. The Hong Kong Observatory is in the city centre of Kowloon and surrounded by high buildings. The airport is located on an artificial island to the north of mountainous Lantau Island. Waglan Island is a small island located to the east of Hong Kong Island. The island is too small to be resolved by the model grid. The WGL station is located 56 m a.s.l. and used as background station by the Hong Kong Observatory. The meteorological parameters are hourly measurements of temperature ( $T$ ), humidity ( $q$ ), sea surface pressure ( $p$ ) and wind ( $v$ ). Temperature and humidity are measured at 2 m above ground level (a.g.l.).

##### 3.1.2 Pearl River Delta Regional Air Quality Monitoring Network

Ground-level NO<sub>2</sub> mixing ratios were provided by the RAQM network. The network was established by the governments of the Guangdong province and Hong Kong to monitor

### Evaluation of a chemistry transport model using a regional OMI NO<sub>2</sub> retrieval

G. Kuhlmann et al.

Title Page

Abstract

Introduction

Conclusions

References

Tables

Figures

◀

▶

◀

▶

Back

Close

Full Screen / Esc

Printer-friendly Version

Interactive Discussion



## Evaluation of a chemistry transport model using a regional OMI NO<sub>2</sub> retrieval

G. Kuhlmann et al.

Title Page

Abstract

Introduction

Conclusions

References

Tables

Figures

◀

▶

◀

▶

Back

Close

Full Screen / Esc

Printer-friendly Version

Interactive Discussion



the air quality in the PRD region and has been in operation since 30 November 2005. It consists of sixteen automatic air quality monitoring stations (see Fig. 1, round markers). The network measures hourly NO<sub>2</sub>, SO<sub>2</sub>, O<sub>3</sub> and PM<sub>10</sub>. The monitoring network was used to validate the NO<sub>2</sub> mixing ratios of the OMI NO<sub>2</sub> products and the CMAQ simulation. In the network, NO<sub>2</sub> was measured by chemiluminescence and DOAS technique with an accuracy and precision of about 10 % (GDEMC and HKEPD, 2006).

### 3.2 CMAQ model simulation

#### 3.2.1 Model run

Three dimensional atmospheric chemistry was simulated in the PRD region for the study period. The simulations were performed with the CMAQ modelling system version 4.7.1 (Byun and Schere, 2006).

Three model domains were defined using a Lambert conformal conic projection (Fig. 1). The coarse domain (D1) covers East Asia with a spatial resolution of 27 km × 27 km. The nested domains have grid resolutions of 9 km × 9 km (D2) and 3 km × 3 km (D3), respectively.

Meteorological fields were provided by the Weather Research and Forecasting (WRF) modelling system (Skamarock et al., 2008) driven by NCEP Final Analysis (FNL) data (NCEP et al., 1997). Horizontal advection was modelled by the mass-conserving YAMO scheme (Yamartino, 1993). The default vertical advection scheme was replaced with the WRF omega calculation with the piecewise parabolic method. The new scheme is the default scheme in CMAQ version 5 and is assumed to provide better vertical profiles. Accurate vertical profiles are important for satellite measurements of air pollutants.

The gas-phase chemistry was modelled by the Euler backward iterative solver optimized for the Carbon Bond-05 mechanism with chlorine (Yarwood et al., 2005). Aerosol chemistry was modelled by the fifth-generation CMAQ aerosol model (aero5) and the impact of clouds on deposition, mixing, photolysis, and aqueous chemistry was de-

scribed by the ACM cloud processor (Pleim and Chang, 1992). Three-dimensional extinction coefficients were computed by the empirical IMPROVE formula (Malm et al., 1994).

The emission inventory used in this simulation was compiled by Du (2008). The inventory combines monthly anthropogenic emission from INTEX-B (Zhang et al., 2009) with biogenic emissions from GEIA (Global Emissions Inventory Activity, Guenther et al., 1995), and biomass burning and ship emissions from TRACE-P (Streets et al., 2003). The INTEX-B emissions were updated with regional emissions for Hong Kong provide by the Hong Kong Environmental Protection Department (Du, 2008). The low-resolution emissions were spatially allocated to each grid cell based on geographic and socio-economic information as well as updated road network and land cover data. Furthermore, weekly and daily cycles were included to the emission inventory (Du, 2008).

### 3.2.2 Data processing

Model outputs are hourly ground level values and three-dimensional fields averaged from 13:00 to 15:00 LT (OMI overpass time).

In addition, at each ground stations, time series of hourly meteorological parameters and  $\text{NO}_2$  mixing ratios were extracted from the model output. The surface pressure in the model was converted to sea level pressure using the simulated temperature. The wind vector in the model was taken at the height of the measurement stations to account for the elevation of the stations above averaged surface height.

Since OMI has a lower spatial resolution than CMAQ, the satellite instrument cannot resolve high-frequency features in the simulated  $\text{NO}_2$  distribution. Therefore, the two datasets were made comparable by averaging the CMAQ data for each OMI ground pixel in an orbit. The pixel boundaries were provided by the overlapping ground pixel product. Within the boundaries, each grid point was weighted based on the instrument's spatial sensitivity (Dobber et al., 2006; Kurosu and Celarier, 2010). Since the set of averaged data is not conveniently visualisable, the CMAQ data were pro-

## Evaluation of a chemistry transport model using a regional OMI $\text{NO}_2$ retrieval

G. Kuhlmann et al.

Title Page

Abstract

Introduction

Conclusions

References

Tables

Figures

◀

▶

◀

▶

Back

Close

Full Screen / Esc

Printer-friendly Version

Interactive Discussion



jected back onto a  $0.01^\circ \times 0.01^\circ$  longitude–latitude grid using a recently developed gridding algorithm (Kuhlmann et al., 2014). The gridding algorithm is available at: <https://github.com/gkuhl/omi>. In this step, missing OMI pixels were also removed from the CMAQ data. Using this approach, the  $\text{NO}_2$  distributions of OMI and CMAQ are directly comparable.

### 3.3 The Hong Kong (HK) OMI $\text{NO}_2$ retrieval

For the HK  $\text{NO}_2$  retrieval, we recalculated tropospheric AMFs by Eq. (2) with new ancillary parameters. The new AMFs were used to compute the tropospheric VCDs by Eq. (1).

For the AMF calculation, a set of ancillary parameters was put together for each OMI ground pixel. The parameters were taken mainly from the WRF/CMAQ simulation. Thus, the retrieval does not depend on any other CTM model which makes the model evaluation easier. The ancillary parameters are surface elevations, temperature, pressure and  $\text{NO}_2$  profiles, and aerosol extinction coefficients. The model domain (D3, Fig. 1) has a spatial resolution of  $3 \text{ km} \times 3 \text{ km}$ . The WRF/CMAQ data were temporally averaged to the OMI overpass time. Further ancillary parameters are cloud height and aerosol/cloud radiance fraction (CRF), which were taken from the OMI  $\text{O}_2\text{--O}_2$  cloud product (Acarreta et al., 2004), and surface reflectance, which was taken from the MODIS MCD43C2 black-sky albedo (BSA) product (Wanner et al., 1997; Lucht et al., 2000). Table 1 compares the updated parameters with the ancillary parameters used in SP2.

All ancillary parameters were projected to a  $0.01^\circ \times 0.01^\circ$  grid and then averaged to each OMI ground pixel. The grid points were weighted based on the instrument's spatial sensitivity within the pixel boundaries, in contrast to other regional retrievals, where each grid point was given equal weight (Russell et al., 2011; Lin et al., 2014).

We recalculated temperature correction coefficients  $\alpha_k(T_k)$ , box AMFs  $m_k$  and partial VCDs  $V_k$ . The temperature correction coefficients  $\alpha_k(T_k)$  were calculated by the empirical Eq. (3) from the WRF/CMAQ output. The box AMFs were computed with the

SCIATRAN radiative transfer model. The partial VCDs were also calculated from the WRF/CMAQ output. As an example, two NO<sub>2</sub> profiles are shown in Fig. 2. In contrast to other regional retrievals, we used three-hour means instead of monthly means.

### 3.3.1 Surface reflectance

The surface reflectance was calculated from the MODIS MCD43C2 BSA product. The product is available every eight days compiled from 16 days of measurements. The spatial resolution is 0.05° × 0.05° (Wanner et al., 1997; Lucht et al., 2000). We calculated the BSAs from the polynomial representation of the bidirectional reflectance distribution function (BRDF) using solar zenith angle (SZA) and model parameters for MODIS Band 3 (Lucht et al., 2000). MODIS Band 3 has a wavelength range from 459 to 479 nm and a centre wavelength of 470 nm. This band is closest to the DOAS fitting window used in the NO<sub>2</sub> retrieval (405–465 nm). Systematic errors due to the wavelength inconsistency are expected to be small. Over water, Lambertian equivalent reflectance (LER) has been reported to decrease from 440 to 470 nm (Kleipool et al., 2008; Zhou et al., 2010). We actually find increased BSA over water surfaces in the PRD region. The MODIS BSA has been used in other regional OMI NO<sub>2</sub> products (Zhou et al., 2010; Russell et al., 2011; Lin et al., 2014).

Since the BSA model parameters have missing values due to cloud contamination, Zhou et al. (2010) filled the data gaps by applying a series of spatial and temporal interpolations. They also reduced measurement noise by applying a smoothing filter. In this work, we combined their steps by using normalised convolution which is a useful algorithm for filling missing values (Knutsson and Westin, 1993). We used a three-dimensional, uniform kernel of size 5 to fill the gaps in the model parameters. To calculate the BSA for each OMI ground pixel, the interpolated BSA model parameters were also projected on the longitude–latitude grid.

## Evaluation of a chemistry transport model using a regional OMI NO<sub>2</sub> retrieval

G. Kuhlmann et al.

Title Page

Abstract

Introduction

Conclusions

References

Tables

Figures

◀

▶

◀

▶

Back

Close

Full Screen / Esc

Printer-friendly Version

Interactive Discussion





**Evaluation of a chemistry transport model using a regional OMI NO<sub>2</sub> retrieval**

G. Kuhlmann et al.

Title Page

Abstract

Introduction

Conclusions

References

Tables

Figures

◀

▶

◀

▶

Back

Close

Full Screen / Esc

Printer-friendly Version

Interactive Discussion



Case 1: No explicit aerosol treatment, i.e. aerosols were only included implicitly through the OMI cloud product.

Case 2: Aerosols were described by the LOWTRAN aerosol parametrization which requires only very limited information about season, aerosols type, visibility and relative humidity at four different layers: planet boundary layer (PBL) (0–2 km), troposphere (2–10 km), stratosphere and mesosphere. We set the season to autumn/winter and the aerosol type to urban. The PBL visibility was calculated from the CMAQ ground extinction coefficients  $\beta$  using the definition of the meteorological optical range (MOR) (World Meteorological Organization, 2008):

$$\text{MOR} = -\frac{\log 0.05}{\beta}. \quad (6)$$

The visibility in the free troposphere was set to 23 km. Furthermore, we assumed that no volcanic aerosols were in the stratosphere or mesosphere. The relative humidity in the PBL and the free troposphere were taken from WRF. Visibility and relative humidity were set to the nearest predefined value in the LOWTRAN parametrisation.

Case 3: Vertical profiles of extinction coefficients  $\beta$  were computed from CMAQ output using the IMPROVE formula. The formula includes a constant Rayleigh extinction coefficient of 0.01 which is subtracted to obtain the aerosol extinction coefficient  $\beta_{\text{ext}}$ . Since the IMPROVE formula calculates  $\beta_{\text{ext}}$  at 550 nm, an Ångström exponent  $\alpha$  for urban aerosols is used to calculate extinction coefficients at 435 nm (Hess et al., 1998). Furthermore, a single scattering albedo  $\omega_0$  of 0.82 (urban aerosol) in PBL (below 2 km) and 0.93 in free troposphere is used to calculate aerosol absorption coefficients  $\beta_{\text{abs}}$ . The phase function is modelled by Henyey–Greenstein parametrisation with an asymmetry factor  $g$  of 0.689 (Hess et al., 1998). As examples, two  $\beta_{\text{ext}}$  profiles are shown in Fig. 2.



## Evaluation of a chemistry transport model using a regional OMI NO<sub>2</sub> retrieval

G. Kuhlmann et al.

Title Page

Abstract

Introduction

Conclusions

References

Tables

Figures

◀

▶

◀

▶

Back

Close

Full Screen / Esc

Printer-friendly Version

Interactive Discussion



Case 4: Since this three parametrisations include aerosols implicitly through the cloud product, aerosol might be counted twice. Therefore, the CRF was corrected by Eq. (5) using the AOT in CMAQ. This was done mainly because recalculation of the OMI cloud product was outside the scope of our study. Since this formula was derived from cloud free observations over North America, generalisation to cloudy pixels in other regions should be considered with great caution. Otherwise, aerosols were treated as in Case 3.

### 3.3.3 Application to OMI SP2

The ancillary parameters were used to calculate new AMFs for all OMI measurements within the PRD region. We created four NO<sub>2</sub> datasets (PRD-1 to PRD-4) for the four aerosol/cloud cases.

While OMI provides daily global coverage, the number of sufficient measurements, which allows for the study of the NO<sub>2</sub> distribution, is limited due to two factors. Firstly, the ground pixel size at the end of the swath is very large and thus not suitable for studying the local spatial distribution. Therefore, only the inner fifty out of sixty rows were used in this study. Secondly, the presence of clouds increases the retrieval uncertainty. Therefore, only ground pixels were used with aerosol/cloud radiance fractions smaller than 50 %. Since the CRF is also sensitive aerosol, this filter criterion is likely to remove heavily polluted days as well.

Based on these filtering constraints, orbits were picked which have a sufficient number of ground pixels to study the spatial distribution of NO<sub>2</sub> in PRD region. The orbits were projected onto a longitude–latitude grid using the same gridding algorithm which has been used to grid the CMAQ data (Kuhlmann et al., 2014).

At each ground stations, time series of NO<sub>2</sub> VCDs were extracted from the data. To study the additive and proportional differences, the OMI VCDs were converted to mixing ratios using the CMAQ NO<sub>2</sub> profile shapes. Since many stations are located on top of buildings, the mixing ratios were calculated at the station height using nearest-neighbour interpolation.

Finally, we used a standard set of typical ancillary parameters (Table 2) to study the impact of the ancillary parameters on the AMF and thus the NO<sub>2</sub> column densities.

## 4 Results and discussions

In this section, we demonstrate and discuss the results of our study. Firstly, we compare briefly the HK retrieval with SP2 to discuss the influence of the updated ancillary parameters. Secondly, we validate the WRF/CMAQ simulation using the RAQM network. Then, we validate the OMI datasets using the RAQM network. Finally, the OMI NO<sub>2</sub> datasets and CMAQ were compared to evaluate the regional chemistry transport model using the HK OMI NO<sub>2</sub> datasets.

### 4.1 OMI regional NO<sub>2</sub> product

In this subsection, we compare the global product (SP2) with our HK retrieval. Only difference relevant for the later discussion in this paper are described here. For a detailed discussion on the different ancillary parameters, we like to refer the reader to earlier studies and reference therein (Zhou et al., 2010; Russell et al., 2011; Lin et al., 2014).

In our study period, 56 days (46 % of all days) with sufficient OMI data were available. Two examples of ungridded NO<sub>2</sub> VCDs are shown in Fig. 3. The spatial distributions are similar for all products but differences can be seen in a pixel-by-pixel comparison. Particularly evident is that the NO<sub>2</sub> VCDs in the HK retrieval have larger maximum values than in the standard product.

The four-month mean NO<sub>2</sub> distributions are shown in Fig. 4c and e. The SP2 has a mean value of  $0.4 \times 10^{16} \text{ cm}^{-2}$ . The mean values in the four datasets range from  $0.6$  to  $0.7 \times 10^{16} \text{ cm}^{-2}$ . The smallest mean value has PRD-1 and the largest has PRD-2. PRD-3 and PRD-4 lie in between these extreme cases. The maximum value in the distribution of SP2 is about  $3.5 \times 10^{16} \text{ cm}^{-2}$  while the HK retrieval datasets have maximum values ranging from  $4.5\text{--}5.5 \times 10^{16} \text{ cm}^{-2}$ .

## Evaluation of a chemistry transport model using a regional OMI NO<sub>2</sub> retrieval

G. Kuhlmann et al.

Title Page

Abstract

Introduction

Conclusions

References

Tables

Figures

◀

▶

◀

▶

Back

Close

Full Screen / Esc

Printer-friendly Version

Interactive Discussion



To study the difference without explicit aerosol treatment we compare SP2 and PRD-1. For this dataset, the VCDs are increased by  $(27 \pm 39)$  %. The difference are due to the updated ancillary parameters, mainly surface reflectance and profile shapes, and thus due to the recalculated AMFs. For SP2, the mean AMF of all available pixels is 1.01 while the mean AMF of PRD-1 is about 17 % smaller (AMF = 0.83).

To quantify the impact of the high-resolution NO<sub>2</sub> profile shapes on the AMF calculation, we compare the CMAQ profiles with an annual GEOS-Chem profile ( $2^\circ \times 2.5^\circ$  spatial resolution) which was used for a satellite validation study in Hong Kong (Chan et al., 2012). The profile was linearly interpolated and extrapolated to the CMAQ vertical levels. The three profiles (see Fig. 2) have been used to compute AMF for the standard case without aerosols (Table 2). The “polluted” CMAQ NO<sub>2</sub> profile has an AMF of 0.82 and is about 3 % smaller than the “clean” profile (AMF = 0.84). The GEOS-Chem profile has an AMF of 1.19 which is 41 % larger than the “clean” and 45 % larger than the “polluted” CMAQ profile. The difference results from the different relative profile shapes. In the CMAQ profiles, the NO<sub>2</sub> number density decreases with altitude, while the GEOS-Chem profile is nearly constant above 2 km. The different profile shapes are related to the different vertical advection schemes used in both models. We expect that the regional CMAQ model provides more accurate vertical distributions than the global GEOS-Chem model. The impact of uncertainties in the profile shapes is difficult to quantify because the uncertainties are not well known due to the lack of NO<sub>2</sub> profile measurements (Boersma et al., 2004). Therefore, we calculated a distribution of AMFs using the simulated profiles at each ground pixel using the standard case. The mean AMF is 0.89 with a SD of 0.08. The largest AMF is 1.64 as a result of an elevated NO<sub>2</sub> layer in the upper troposphere. The smallest AMF is 0.75 which is 16 % smaller than the mean AMF. The small AMF is the result of a heavily polluted ground layer. In summary, the AMF for the high-resolution profiles is about  $(35 \pm 11)$  % smaller than the low-resolution profile.

The profile shapes can also be used to convert VCDs to number concentrations or mixing ratios. For the standard case, the mean conversion factor ( $V_0/(\Delta z_0 V_{\text{trop}})$ )





land (HKO and HKIA). The model also overestimates humidity on Waglan Island where the model data are at the sea surface while measurements were taken at station height of 56 m over the sea surface.

Since the wind field is impacted strongly by local topography, the agreement between model and observation is normally lower where the topography is complex and thus cannot be resolved by the model. The Hong Kong Observatory uses Waglan Island as reference station because it is not influenced by local topography. The agreement between model and observations on Waglan Island is good (IOA = 0.84). At HKIA the wind field is impacted by the mountainous Lantau Island and thus the agreement is lower (IOA = 0.68). The HKO station is located within urbanised Kowloon and surrounded by high buildings. Consequently, the agreement between model and observations is low (IOA = 0.57).

The evaluation of the meteorological fields shows good agreement between model and observations within the expected limitations due to the model resolution. The agreement is lower for the wind fields due to the impact of local topography. Unfortunately no meteorological data for the whole PRD region were available for this analysis. However, due to the high agreement in Hong Kong, similar model performance is expected in the complete model domain. The meteorological fields are sufficient to provide input for the chemistry transport simulations.

#### 4.2.2 NO<sub>2</sub> mixing ratios

The results of the statistical evaluation between CMAQ and RAQM network are summarised in the Supplement. At the sixteen stations, the index of agreements vary between 0.29 and 0.75. At most stations the IOA is about 0.5. At Tap Mun, the low IOA is the result of several peaks in the simulated time series which are not found in the measurements. The peaks were traced back to NO<sub>x</sub> emissions at the Dapend Peninsula about 15 km east of Tap Mun (not shown). Other stations in Hong Kong have IOA above average.

## Evaluation of a chemistry transport model using a regional OMI NO<sub>2</sub> retrieval

G. Kuhlmann et al.

Title Page

Abstract

Introduction

Conclusions

References

Tables

Figures

◀

▶

◀

▶

Back

Close

Full Screen / Esc

Printer-friendly Version

Interactive Discussion



## Evaluation of a chemistry transport model using a regional OMI NO<sub>2</sub> retrieval

G. Kuhlmann et al.

Title Page

Abstract

Introduction

Conclusions

References

Tables

Figures

◀

▶

◀

▶

Back

Close

Full Screen / Esc

Printer-friendly Version

Interactive Discussion



There are various reasons for the disagreement between model and measurements. Firstly, the point measurement may not be representative for the grid cell because of the influence of local sources and sinks. Secondly, local topography and station height can also impact the NO<sub>2</sub> mixing ratios. On the other hand, the differences can arise from the model due to the limited parametrisation of the chemistry and in particular the insufficient knowledge of the strength and distribution of the emissions.

The average ground mixing ratios are shown in Fig. 7. In the observations, two major plumes can be identified at Hong Kong and Shenzhen (HK & SZ), which includes the network stations Liyuan, Tap Mun, Tung Chung and Tsuen Wan, and Foshan and Guangzhou (FS & GZ), which includes the stations Huijingcheng, Luhu Park, Shunde Dangxia and Wanqingsha. The latter plume cannot be found in the simulations. The mean bias is close to zero (−5%) at the stations in HK & SZ. The bias is larger in FS & GZ with a MB of −17.6 ppbv (−45%).

The better agreement over Hong Kong is thought to be the result of the updated emission inventory with local information from Hong Kong which are more accurate. The low agreement between model and observation is not very satisfying. In another study, Wu et al. (2012) evaluated CMAQ in the PRD region using a similar emission inventory and reported similar CVs (see Appendix A for definition) and normalised mean biases. The low model performance can impact the quality of the OMI NO<sub>2</sub> dataset because the low model performance might reduce the accuracy of the NO<sub>2</sub> profile shape and thus impact the air mass factor and the conversion factor which is used to convert VCDs to ground mixing ratios.

### 4.3 OMI validation with ground measurements

In this subsection, OMI NO<sub>2</sub> columns were compared with the RAQM network. The validation with point measurements is challenging, because OMI measures the mean value within the ground pixels (at least 13 km × 24 km). Since NO<sub>2</sub> has a high spatial variability, area average and point measurement may not agree well; in particular in an urban area with complex NO<sub>2</sub> sources and sinks. Furthermore, if the VCDs are

converted to ground values with the CMAQ profile shapes, the validation depends on the modelled NO<sub>2</sub> profiles which can have large uncertainties.

In order to get an idea for the expected deviations, we compared the time series of the processed CMAQ data, which have been averaged to the OMI ground pixels, with the raw CMAQ data (3 km × 3 km) at the 16 stations. Table 4 shows the mean error measures for all stations and for the stations within the two plumes. The correlation coefficient is low, in particular, over HK & SZ. This lower agreement in Hong Kong could result from the complex terrain along the coastline and the strong gradient between clean and polluted air (see Fig. 7a). Against that, the NO<sub>2</sub> distribution in FS & GZ is smoother. Table 4 also shows that the processed data have lower mixing ratios with a mean bias between -10 and -20% which is the result of the spatial averaging. The generalisation of these results to the OMI validation should be done with caution because it requires that the model simulates the spatial distribution on a small scale accurately. Nonetheless, this analysis provides some useful information on the expected deviations between satellite and ground measurements.

To study additive and proportional differences between satellite and ground measurements, the OMI VCDs were converted to ground level mixing ratios using the CMAQ NO<sub>2</sub> profile shapes. As an example, the ground mixing ratio distribution for 29 January 2007 is shown in Fig. 8 using a “standard” and the newly developed gridding algorithm. The new algorithm creates continuous distributions which is helpful for the study of the spatial distribution distribution. It should be noted that the high-resolution features are the result of modelled profile shapes. Therefore, the ground mixing ratios depend strongly on the NO<sub>2</sub> profile shape in the model.

Table 5 shows the statistical measures for the comparison between OMI and the ground network for SP2 and datasets using the HK retrieval. The correlation coefficients are similar for all datasets. The size of the correlation coefficient is comparable to the expected values (Table 4). The correlation coefficients is slightly smaller at FS & GZ which is likely related to the low model performance in this area.

**Evaluation of a chemistry transport model using a regional OMI NO<sub>2</sub> retrieval**

G. Kuhlmann et al.

Title Page

Abstract Introduction

Conclusions References

Tables Figures

◀ ▶

◀ ▶

Back Close

Full Screen / Esc

Printer-friendly Version

Interactive Discussion





## Evaluation of a chemistry transport model using a regional OMI NO<sub>2</sub> retrieval

G. Kuhlmann et al.

Title Page

Abstract

Introduction

Conclusions

References

Tables

Figures

◀

▶

◀

▶

Back

Close

Full Screen / Esc

Printer-friendly Version

Interactive Discussion



There are large differences between the mean biases. The bias is largest for the global product (SP2). In the HK retrieval, the mean bias depends on the amount of aerosols. The bias is largest for PRD-1 and smallest for PRD-2, while PRD-3 and 4 lie in between them. The magnitude of the bias is closest to the expected value for PRD-4.

The reduced mean bias is an important improvement of the HK NO<sub>2</sub> retrieval.

Table 6 shows the mean values of CMAQ, OMI datasets and RAQM network at the location of the 16 stations. If the local NO<sub>2</sub> distribution was simulated perfectly, the raw CMAQ data would agree with the network measurements and the processed CMAQ data would agree with the OMI measurements. However, the bias between OMI PRD-4 and RAQM network at FS & GZ is larger than the expected value. The difference is likely the result of the CMAQ model bias in this area. If we compare the “clean” and “polluted” standard case (Table 2), the different profile shape (−3%), conversion factor (−3%) and the influence of the aerosols (−10%) can increase the AMF by 10 to 20% (see Sect. 4.1). As a result, the OMI NO<sub>2</sub> VCDs would be larger and the bias between OMI and network would become smaller.

To conclude, the correlation coefficient between all OMI datasets and ground measurements is low. The low correlation is mainly related to the OMI ground pixel size as well as to the unsatisfactory performance of the CMAQ model. However, the HK retrieval reduces the mean bias between satellite and ground measurements significantly. The larger bias in FS & GZ suggests that OMI VCDs might be still underestimated in the HK retrieval (PRD-4) due to the model bias in this region.

#### 4.4 CMAQ evaluation with OMI NO<sub>2</sub> datasets in the model domain

In this subsection, we compare the OMI datasets with the CMAQ data. We discuss mainly PRD-4 which performed best in the validation with ground measurements. Since the correlation between OMI and RAQM network is low, only spatially or temporally averaged distribution were compared which reduces the random noise.

Figure 4a–c and e shows the four-month averaged CMAQ and OMI NO<sub>2</sub> VCDs. The averaged raw CMAQ data and the processed CMAQ data are shown Fig. 4a and b.



## 5 Discussions and conclusions

In this paper, we evaluate a regional CTM (3 km × 3 km spatial resolution) with satellite measurements. We simulated three-dimensional atmospheric chemistry with the CMAQ modelling system the PRD region from October 2006 to January 2007. Furthermore, we developed a new OMI NO<sub>2</sub> retrieval for this region. The CMAQ model was evaluated with the global OMI NO<sub>2</sub> standard product (SP2), our HK NO<sub>2</sub> retrieval using different aerosol parametrizations (PRD-1 to PRD-4), and ground measurements of the PRD Regional Air Quality Monitoring (RAQM) network.

In the HK retrieval, we recalculated tropospheric AMFs using updated ancillary parameters of NO<sub>2</sub> profile shapes, surface reflectance and aerosol profiles. Our best retrieval (PRD-4) increases the NO<sub>2</sub> VCDs by (+31 ± 38) %, when compared to SP2, and thus reduces the mean bias between satellite and ground measurements significantly (−15 % instead of −41 %). The differences are due to changes in the ancillary parameters used for the AMF calculation. These parameters are NO<sub>2</sub> profile shapes (−35 ± 11) %, surface reflectance (−5 to −10 %) and aerosols (−8 to 14 %). The remaining difference between satellite and ground measurements can be explained by the area averaging due to the OMI ground pixel size and by the CMAQ model bias because the OMI NO<sub>2</sub> retrieval depends on the CMAQ model output. As a result, if the CMAQ model underestimates NO<sub>2</sub> mixing ratios or aerosols, the OMI VCDs can be underestimated as well. This relation should be considered in an evaluation study.

In a polluted environment, accurate knowledge of the vertical profiles of aerosol and cloud scattering as well as NO<sub>2</sub> profile shapes are important to calculate accurate column densities. Our study is limited by unquantified errors due to uncertainties in the NO<sub>2</sub> profile and aerosol profile. In future studies, the HK retrieval should be reviewed by validating the CMAQ NO<sub>2</sub> profiles. Furthermore, the aerosol optical properties were calculated by the IMPROVE formula which has not been developed to calculate profiles in an urban environment. However, the IMPROVE formula can be improved for such an application (Zhang et al., 2013) which we like to include in a future version.

## Evaluation of a chemistry transport model using a regional OMI NO<sub>2</sub> retrieval

G. Kuhlmann et al.

Title Page

Abstract

Introduction

Conclusions

References

Tables

Figures

◀

▶

◀

▶

Back

Close

Full Screen / Esc

Printer-friendly Version

Interactive Discussion



Otherwise, optical properties can be calculated by Mie theory. The aerosol information can be improved further by validating them with ground- or satellite-based products. A third aspect is the impact of clouds which need to be studied more in future. Satellite products, which provide a clean separation between aerosols, clouds and surface reflectance, are desirable, because this would allow to use different data sources for these ancillary parameters.

The performance of the model is not very satisfying. The correlation between CMAQ and RAQM network is low ( $r \approx 0.3$ ) and the model underestimates the NO<sub>2</sub> concentrations in the north-western model domain (Foshan and Guangzhou). The low performance is assumed to be associated with the used emissions inventory, because the model performance is better in Hong Kong and Shenzhen where the emission inventory has been updated with local data. The model evaluation with the HK retrieval (PRD-4) gives similar results. In Hong Kong and Shenzhen, the model overestimates the NO<sub>2</sub> VCDs by about 15 %, while the correlation coefficient is satisfactory ( $r = 0.56$ ). In Foshan and Guangzhou, the correlation is low ( $r = 0.37$ ) and the model underestimates the VCDs strongly (MB = -40 %). Furthermore, we estimated that the HK retrieval also underestimated VCDs by about 10 to 20 % in Foshan and Guangzhou because of the influence of the model parameters on the AMF. The results of both model evaluations with the RAQM network and the datasets created by the HK algorithm are consistent.

To conclude, our study demonstrates that the datasets created by the HK retrieval are suitable for the evaluation of the spatial distribution and the magnitude of NO<sub>2</sub> concentrations in the model. We showed that a retrieval, which updates not only the profile shapes, reduces the OMI bias over urban areas. In future studies, easy-to-use tools need to be developed which allow such evaluations of CTMs with satellite measurements as easy as using ground network measurements.

### Appendix A: Error measures

The following measures are used to compare observations and model:

- Index of agreement (Willmott, 1981):

$$\text{IOA} = 1 - \frac{\sum_{i=1}^N (x_i - y_i)^2}{\sum_{i=1}^N (|x_i - \langle y \rangle| + |y_i - \langle y \rangle|)^2} \quad (\text{A1})$$

where  $\langle \cdot \rangle$  is the mean value.

- Pearson's correlation coefficient:

$$r = \frac{1}{n-1} \sum_{i=1}^N \left( \frac{y_i - \langle y \rangle}{\sigma_y} \right) \left( \frac{x_i - \langle x \rangle}{\sigma_x} \right) \quad (\text{A2})$$

$\sigma_x$  and  $\sigma_y$  are sample SDs.

- Root mean square error:

$$\text{RMSE} = \sqrt{\frac{1}{N} \sum_{i=1}^N (x_i - y_i)^2}. \quad (\text{A3})$$

- Coefficient of variation of the RMSE:

$$\text{CV} = \frac{\text{RMSE}}{\langle y \rangle}. \quad (\text{A4})$$

- Mean bias:

$$\text{MB} = \frac{1}{N} \sum_{i=1}^N (x_i - y_i). \quad (\text{A5})$$

- Normalised mean bias:

$$\text{NMB} = \frac{\text{MB}}{\langle y \rangle}. \quad (\text{A6})$$

31067

**Evaluation of a chemistry transport model using a regional OMI NO<sub>2</sub> retrieval**

G. Kuhlmann et al.

Title Page

Abstract

Introduction

Conclusions

References

Tables

Figures

◀

▶

◀

▶

Back

Close

Full Screen / Esc

Printer-friendly Version

Interactive Discussion



*Acknowledgements.* The work described in this paper is partly funded by the Guy Carpenter Asia-Pacific Climate Impact Centre (project no. 9360126), a grant from the Research Grant Council of Hong Kong (project no. 102912) and the start-up grant from City University of Hong Kong (project no. 7200296).

## References

- Acarreta, J. R., De Haan, J. F., and Stammes, P.: Cloud pressure retrieval using the O<sub>2</sub>-O<sub>2</sub> absorption band at 477 nm, *J. Geophys. Res.*, 109, D05204, doi:10.1029/2003JD003915, 2004. 31043, 31046, 31051
- Bey, I., Jacob, D. J., Yantosca, R. M., Logan, J. A., Field, B. D., Fiore, A. M., Li, Q., Liu, H. Y., Mickley, L. J., and Schultz, M. G.: Global modeling of tropospheric chemistry with assimilated meteorology: model description and evaluation, *J. Geophys. Res.*, 106, 23073–23095, doi:10.1029/2001JD000807, 2001. 31047
- Boersma, K. F., Eskes, H. J., and Brinksma, E. J.: Error analysis for tropospheric NO<sub>2</sub> retrieval from space, *J. Geophys. Res.*, 109, D04311, doi:10.1029/2003JD003962, 2004. 31053, 31057
- Boersma, K. F., Eskes, H. J., Meijer, E. W., and Kelder, H. M.: Estimates of lightning NO<sub>x</sub> production from GOME satellite observations, *Atmos. Chem. Phys.*, 5, 2311–2331, doi:10.5194/acp-5-2311-2005, 2005. 31043
- Boersma, K. F., Eskes, H. J., Veefkind, J. P., Brinksma, E. J., van der A, R. J., Sneep, M., van den Oord, G. H. J., Levelt, P. F., Stammes, P., Gleason, J. F., and Bucsela, E. J.: Near-real time retrieval of tropospheric NO<sub>2</sub> from OMI, *Atmos. Chem. Phys.*, 7, 2103–2118, doi:10.5194/acp-7-2103-2007, 2007. 31041, 31042
- Boersma, K. F., Eskes, H. J., Dirksen, R. J., van der A, R. J., Veefkind, J. P., Stammes, P., Huijnen, V., Kleipool, Q. L., Sneep, M., Claas, J., Leitão, J., Richter, A., Zhou, Y., and Brunner, D.: An improved tropospheric NO<sub>2</sub> column retrieval algorithm for the Ozone Monitoring Instrument, *Atmos. Meas. Tech.*, 4, 1905–1928, doi:10.5194/amt-4-1905-2011, 2011. 31042, 31053

Evaluation of a chemistry transport model using a regional OMI NO<sub>2</sub> retrieval

G. Kuhlmann et al.

Title Page

Abstract

Introduction

Conclusions

References

Tables

Figures

◀

▶

◀

▶

Back

Close

Full Screen / Esc

Printer-friendly Version

Interactive Discussion



**Evaluation of a chemistry transport model using a regional OMI NO<sub>2</sub> retrieval**

G. Kuhlmann et al.

Title Page

Abstract

Introduction

Conclusions

References

Tables

Figures

◀

▶

◀

▶

Back

Close

Full Screen / Esc

Printer-friendly Version

Interactive Discussion



Bovensmann, H., Burrows, J. P., Buchwitz, M., Frerick, J., Noël, S., Rozanov, V. V., Chance, K. V., and Goede, A. P. H.: SCIAMACHY: mission objectives and measurement modes, *J. Atmos. Sci.*, 56, 127–150, 1999. 31041

Bucsela, E. J., Celarier, E. A., Wenig, M. O., Gleason, J. F., Veefkind, J. P., Boersma, K. F., and Brinksma, E. J.: Algorithm for NO<sub>2</sub> vertical column retrieval from the ozone monitoring instrument, *IEEE T. Geosci. Remote*, 44, 1245–1258, doi:10.1109/TGRS.2005.863715, 2006. 31041, 31045

Bucsela, E. J., Krotkov, N. A., Celarier, E. A., Lamsal, L. N., Swartz, W. H., Bhartia, P. K., Boersma, K. F., Veefkind, J. P., Gleason, J. F., and Pickering, K. E.: A new stratospheric and tropospheric NO<sub>2</sub> retrieval algorithm for nadir-viewing satellite instruments: applications to OMI, *Atmos. Meas. Tech.*, 6, 2607–2626, doi:10.5194/amt-6-2607-2013, 2013. 31041, 31045, 31046, 31047

Burrows, J. P., Weber, M., Buchwitz, M., Rozanov, V., Ladstätter-Weißenmayer, A., Richter, A., DeBeek, R., Hoogen, R., Bramstedt, K., Eichmann, K. U., Eisinger, M. and Perner, D.: The global ozone monitoring experiment (GOME): mission concept and first scientific results, *J. Atmos. Sci.*, 56, 151–175, 1999. 31041

Byun, D. and Schere, K. L.: Review of the governing equations, computational algorithms, and other components of the Models-3 Community Multiscale Air Quality (CMAQ) modeling system, *Appl. Mech. Rev.*, 59, 51–57, doi:10.1115/1.2128636, 2006. 31043, 31049

Callies, J., Corpaccioli, E., Eisinger, M., Hahne, A., and Lefebvre, A.: GOME-2 – Metop's second-generation sensor for operational ozone monitoring, *ESA Bull.-Eur. Space*, 102, 28–36, 2000. 31041

Chan, K. L., Pöhler, D., Kuhlmann, G., Hartl, A., Platt, U., and Wenig, M. O.: NO<sub>2</sub> measurements in Hong Kong using LED based long path differential optical absorption spectroscopy, *Atmos. Meas. Tech.*, 5, 901–912, doi:10.5194/amt-5-901-2012, 2012. 31057

Dave, J. V.: Multiple scattering in a non-homogeneous, Rayleigh atmosphere, *J. Atmos. Sci.*, 22, 273–279, 1965. 31046

Dobber, M., Dirksen, R., Levelt, P., Van den Oord, G. H. J., Voors, R., Kleipool, Q., Jaross, G., Kowalewski, M., Hilsenrath, E., Leppelmeier, G., de Vries, J., Dierssen, W., and Rozemeijer, N.: Ozone monitoring instrument calibration, *IEEE T. Geosci. Remote*, 44, 1209–1238, doi:10.1109/TGRS.2006.869987, 2006. 31050

**Evaluation of a chemistry transport model using a regional OMI NO<sub>2</sub> retrieval**

G. Kuhlmann et al.

Title Page

Abstract

Introduction

Conclusions

References

Tables

Figures

◀

▶

◀

▶

Back

Close

Full Screen / Esc

Printer-friendly Version

Interactive Discussion

- Douglass, A. R., Stolarski, R. S., Strahan, S. E., and Connell, P. S.: Radicals and reservoirs in the GMI chemistry and transport model: comparison to measurements, *J. Geophys. Res.*, 109, D16302, doi:10.1029/2004JD004632, 2004. 31047
- Driscoll, C. T., Lawrence, G. B., Bulger, A. J., Butler, T. J., Cronan, C. S., Eagar, C., Lambert, K. F., Likens, G. E., Stoddard, J. L., and Weathers, K.: Acidic deposition in the north-eastern United States: sources and inputs, ecosystem effects, and management strategies, *Bioscience*, 51, 180–198, doi:10.1641/0006-3568(2001)051[0180:ADITNU]2.0.CO;2, 2001. 31041
- Du, Y.: New consolidation of emission and processing for air quality modeling assessment in Asia, Master's thesis, University of Tennessee, available at: [http://trace.tennessee.edu/utk\\_gradthes/372](http://trace.tennessee.edu/utk_gradthes/372) (last access: August 2014), 2008. 31050
- Duncan, B. N., Strahan, S. E., Yoshida, Y., Steenrod, S. D., and Livesey, N.: Model study of the cross-tropopause transport of biomass burning pollution, *Atmos. Chem. Phys.*, 7, 3713–3736, doi:10.5194/acp-7-3713-2007, 2007. 31047
- Eskes, H. J. and Boersma, K. F.: Averaging kernels for DOAS total-column satellite retrievals, *Atmos. Chem. Phys.*, 3, 1285–1291, doi:10.5194/acp-3-1285-2003, 2003. 31043
- Guangdong Provincial Environmental Protection Monitoring Centre (GDEMC) and Environmental Protection Department, HKSAR (HKEPD): Pearl River Delta Regional Air Quality Monitoring Network – a report of monitoring results in 2006 (PRDAIR-2006-2), available at: [http://www.epd.gov.hk/epd/english/resources\\_pub/publications/m\\_report.html](http://www.epd.gov.hk/epd/english/resources_pub/publications/m_report.html) (last access: April 2014), 2006. 31049
- Guenther, A., Hewitt, C. N., Erickson, D., Fall, R., Geron, C., Graedel, T., Harley, P., Klinger, L., Lerdau, M., McKay, W. A., Pierce, T., Scholes, B., Steinbrecher, R., Tallamraju, R., Taylor, J., and Zimmerman, P.: A global model of natural volatile organic compound emissions, *J. Geophys. Res.*, 100, 8873–8892, doi:10.1029/94JD02950, 1995. 31050
- Haagen-Smit, A. J.: Chemistry and physiology of Los Angeles smog, *Ind. Eng. Chem.*, 44, 1342–1346, 1952. 31041
- Han, K. M., Lee, C. K., Lee, J., Kim, J., and Song, C. H.: A comparison study between model-predicted and OMI-retrieved tropospheric NO<sub>2</sub> columns over the Korean peninsula, *Atmos. Environ.*, 45, 2962–2971, doi:10.1016/j.atmosenv.2010.10.016, 2011. 31043
- He, Q., Li, C., Mao, J., Lau, A. K.-H., and Chu, D. A.: Analysis of aerosol vertical distribution and variability in Hong Kong, *J. Geophys. Res.*, 113, D14211, doi:10.1029/2008JD009778, 2008. 31059



---

**Evaluation of a chemistry transport model using a regional OMI NO<sub>2</sub> retrieval**G. Kuhlmann et al.

---

[Title Page](#)[Abstract](#)[Introduction](#)[Conclusions](#)[References](#)[Tables](#)[Figures](#)[◀](#)[▶](#)[◀](#)[▶](#)[Back](#)[Close](#)[Full Screen / Esc](#)[Printer-friendly Version](#)[Interactive Discussion](#)

Herron-Thorpe, F. L., Lamb, B. K., Mount, G. H., and Vaughan, J. K.: Evaluation of a regional air quality forecast model for tropospheric NO<sub>2</sub> columns using the OMI/Aura satellite tropospheric NO<sub>2</sub> product, *Atmos. Chem. Phys.*, 10, 8839–8854, doi:10.5194/acp-10-8839-2010, 2010. 31043

5 Hess, M., Koepke, P., and Schult, I.: Optical properties of aerosols and clouds: the software package OPAC, *B. Am. Meteorol. Soc.*, 79, 831–844, 1998. 31054

Kleipool, Q. L., Dobber, M. R., de Haan, J. F., and Levelt, P. F.: Earth surface reflectance climatology from 3 years of OMI data, *J. Geophys. Res.*, 113, D18308, doi:10.1029/2008JD010290, 2008. 31052, 31053

10 Knutsson, H. and Westin, C.-F.: Normalized and differential convolution: methods for interpolation and filtering of incomplete and uncertain data, in: *Proceedings of Computer Vision and Pattern Recognition ('93)*, New York City, USA, 16–19 June 1993, 515–523, 1993. 31052

Kuhlmann, G., Hartl, A., Cheung, H. M., Lam, Y. F., and Wenig, M. O.: A novel gridding algorithm to create regional trace gas maps from satellite observations, *Atmos. Meas. Tech.*, 7, 451–467, doi:10.5194/amt-7-451-2014, 2014. 31051, 31055, 31089

15 Kurosu, T. P. and Celarier, E. A.: OMPIXCOR Readme File, available at: [http://disc.sci.gsfc.nasa.gov/Aura/data-holdings/OMI/documents/v003/OMPIXCOR\\_README\\_V003.pdf](http://disc.sci.gsfc.nasa.gov/Aura/data-holdings/OMI/documents/v003/OMPIXCOR_README_V003.pdf) (last access: August 2014), 2010. 31050

Levelt, P., van den Oord, G., Dobber, M., Malkki, A., Visser, H., de Vries, J., Stammes, P., 20 Lundell, J., and Saari, H.: The ozone monitoring instrument, *IEEE T. Geosci. Remote*, 44, 1093–1101, doi:10.1109/TGRS.2006.872333, 2006. 31041, 31044

Lin, J.-T., Martin, R. V., Boersma, K. F., Sneep, M., Stammes, P., Spurr, R., Wang, P., Van Roozendaal, M., Clémer, K., and Irie, H.: Retrieving tropospheric nitrogen dioxide from the Ozone Monitoring Instrument: effects of aerosols, surface reflectance anisotropy, and vertical profile of nitrogen dioxide, *Atmos. Chem. Phys.*, 14, 1441–1461, doi:10.5194/acp-14-1441-2014, 2014. 31042, 31051, 31052, 31053, 31056

25 Lucht, W., Schaaf, C., and Strahler, A.: An algorithm for the retrieval of albedo from space using semiempirical BRDF models, *IEEE T. Geosci. Remote*, 38, 977–998, doi:10.1109/36.841980, 2000. 31044, 31051, 31052

30 Malm, W., Gebhart, K., Molenaar, J., Cahill, T., Eldred, R., and Huffman, D.: Examining the relationship between atmospheric aerosols and light extinction at Mount Rainier and North Cascades National Parks, *Atmos. Environ.*, 28, 347–360, doi:10.1016/1352-2310(94)90110-4, 1994. 31050, 31053



**Evaluation of a chemistry transport model using a regional OMI NO<sub>2</sub> retrieval**

G. Kuhlmann et al.

Title Page

Abstract

Introduction

Conclusions

References

Tables

Figures

◀

▶

◀

▶

Back

Close

Full Screen / Esc

Printer-friendly Version

Interactive Discussion

Solomon, S., Schmeltekopf, A., and Sanders, R.: On the interpretation of zenith sky absorption measurements, *J. Geophys. Res.*, 92, 8311–8319, doi:10.1029/JD092iD07p08311, 1987. 31045

Strahan, S. E., Duncan, B. N., and Hoor, P.: Observationally derived transport diagnostics for the lowermost stratosphere and their application to the GMI chemistry and transport model, *Atmos. Chem. Phys.*, 7, 2435–2445, doi:10.5194/acp-7-2435-2007, 2007. 31047

Streets, D. G., Bond, T. C., Carmichael, G. R., Fernandes, S. D., Fu, Q., He, D., Klimont, Z., Nelson, S. M., Tsai, N. Y., Wang, M. Q., Woo, J.-H., and Yarber, K. F.: An inventory of gaseous and primary aerosol emissions in Asia in the year 2000, *J. Geophys. Res.*, 108, 8809, doi:10.1029/2002JD003093, 2003. 31050

Wanner, W., Strahler, A. H., Hu, B., Lewis, P., Muller, J.-P., Li, X., Schaaf, C. L. B., and Barnsley, M. J.: Global retrieval of bidirectional reflectance and albedo over land from EOS MODIS and MISR data: theory and algorithm, *J. Geophys. Res.*, 102, 17143–17161, doi:10.1029/96JD03295, 1997. 31044, 31051, 31052

Willmott, C. J.: On the validation of models, *Phys. Geogr.*, 2, 184–194, <http://www.tandfonline.com/doi/abs/10.1080/02723646.1981.10642213>, 1981. 31067

World Meteorological Organization: WMO Guide to Meteorological Instruments and Methods of Observation, World Meteorological Organization, 7th edn., Geneva, 2008. 31054

Wu, Q., Wang, Z., Chen, H., Zhou, W., and Wenig, M.: An evaluation of air quality modeling over the Pearl River Delta during November 2006, *Meteorol. Atmos. Phys.*, 116, 113–132, doi:10.1007/s00703-011-0179-z, 2012. 31061

Yamartino, R. J.: Nonnegative, conserved scalar transport using grid-cell-centered, spectrally constrained Blackman cubics for applications on a variable-thickness mesh, *Mon. Weather Rev.*, 121, 753–763, doi:10.1175/1520-0493(1993)121<0753:NCSTUG>2.0.CO;2, 1993. 31049

Yarwood, G., Rao, S., Yocke, M., and Whitten, G. Z.: Updates to the Carbon Bond chemical mechanism: CB05. Final Report to the U.S. EPA, RT-0400675, available at: [http://www.camx.com/publ/pdfs/cb05\\_final\\_report\\_120805.pdf](http://www.camx.com/publ/pdfs/cb05_final_report_120805.pdf) (last access: February 2014), 2005. 31049

Zhang, Q., Streets, D. G., Carmichael, G. R., He, K. B., Huo, H., Kannari, A., Klimont, Z., Park, I. S., Reddy, S., Fu, J. S., Chen, D., Duan, L., Lei, Y., Wang, L. T., and Yao, Z. L.: Asian emissions in 2006 for the NASA INTEX-B mission, *Atmos. Chem. Phys.*, 9, 5131–5153, doi:10.5194/acp-9-5131-2009, 2009. 31050

**Evaluation of a chemistry transport model using a regional OMI NO<sub>2</sub> retrieval**

G. Kuhlmann et al.

[Title Page](#)[Abstract](#)[Introduction](#)[Conclusions](#)[References](#)[Tables](#)[Figures](#)[◀](#)[▶](#)[◀](#)[▶](#)[Back](#)[Close](#)[Full Screen / Esc](#)[Printer-friendly Version](#)[Interactive Discussion](#)

- Zhang, R., Bian, Q., Fung, J. C., and Lau, A. K.: Mathematical modeling of seasonal variations in visibility in Hong Kong and the Pearl River Delta region, *Atmos. Environ.*, 77, 803–816, doi:10.1016/j.atmosenv.2013.05.048, 2013. 31065
- 5 Zhou, Y., Brunner, D., Boersma, K. F., Dirksen, R., and Wang, P.: An improved tropospheric NO<sub>2</sub> retrieval for OMI observations in the vicinity of mountainous terrain, *Atmos. Meas. Tech.*, 2, 401–416, doi:10.5194/amt-2-401-2009, 2009. 31042
- Zhou, Y., Brunner, D., Spurr, R. J. D., Boersma, K. F., Sneep, M., Popp, C., and Buchmann, B.: Accounting for surface reflectance anisotropy in satellite retrievals of tropospheric NO<sub>2</sub>, *Atmos. Meas. Tech.*, 3, 1185–1203, doi:10.5194/amt-3-1185-2010, 2010. 31042, 31052, 31056
- 10 Zyrichidou, I., Koukouli, M. E., Balis, D. S., Kioutsoukis, I., Poupkou, A., Katragkou, E., Melas, D., Boersma, K., and van Roozendael, M.: Evaluation of high resolution simulated and OMI retrieved tropospheric NO<sub>2</sub> column densities over Southeastern Europe, *Atmos. Res.*, 122, 55–66, doi:10.1016/j.atmosres.2012.10.028, 2013. 31043

## Evaluation of a chemistry transport model using a regional OMI NO<sub>2</sub> retrieval

G. Kuhlmann et al.

Title Page

Abstract

Introduction

Conclusions

References

Tables

Figures

◀

▶

◀

▶

Back

Close

Full Screen / Esc

Printer-friendly Version

Interactive Discussion



**Table 1.** Ancillary parameters used for deriving tropospheric NO<sub>2</sub> column densities from OMI.

	Standard Product (SP2)	HK Retrieval (this work)
surface reflectance	OMI LER (5 year, monthly climatology, 0.5° × 0.5°)	MODIS MCD43C2 black-sky albedo (every 8 days, 0.05° × 0.05°)
surface pressure	GMI (2° × 2.5°, adjusted for elevation)	WRF (3 km × 3 km)
cloud pressure and fraction	OMI O <sub>2</sub> –O <sub>2</sub> cloud algorithm	OMI O <sub>2</sub> –O <sub>2</sub> cloud algorithm
aerosol optics	implicit	CMAQ (3 km × 3 km)
NO <sub>2</sub> profile shapes	GMI (multi-year monthly climatology, 2° × 2.5°)	CMAQ (3 km × 3 km)
temperature profiles	GEOS-5 (monthly)	WRF (3 km × 3 km)
RTM	TOMRAD	SCIATRAN
AMF calculation	interpolated from a look-up table	pixel-specific (no look-up table)
pixel sensitivity	centre point	instrument function

## Evaluation of a chemistry transport model using a regional OMI NO<sub>2</sub> retrieval

G. Kuhlmann et al.

Title Page

Abstract

Introduction

Conclusions

References

Tables

Figures

◀

▶

◀

▶

Back

Close

Full Screen / Esc

Printer-friendly Version

Interactive Discussion



**Table 2.** Standard set of ancillary parameters used in the AMF sensitivity study.

Ancillary Parameter	Value
solar zenith angle (SZA)	48°
viewing zenith angle (VZA)	0° (nadir)
relative azimuth angle (RAA)	180°
terrain height	0.0 km
surface reflectance	0.05
aerosol/cloud radiance fraction	0.00
temperature and pressure profiles	WRF average
NO <sub>2</sub> and aerosol profiles	CMAQ averages (see Fig. 2)

## Evaluation of a chemistry transport model using a regional OMI NO<sub>2</sub> retrieval

G. Kuhlmann et al.

**Table 3.** The AMFs for different aerosol treatment cases for the standard parameters and profiles (Fig. 2).

	PRD-1	PRD-2		PRD-3 & 4	
		clean	polluted	clean	polluted
NO <sub>2</sub> clean	0.84	0.68	0.39	0.77	0.74
NO <sub>2</sub> polluted	0.82	0.65	0.35	0.74	0.70

[Title Page](#)[Abstract](#)[Introduction](#)[Conclusions](#)[References](#)[Tables](#)[Figures](#)[⏪](#)[⏩](#)[◀](#)[▶](#)[Back](#)[Close](#)[Full Screen / Esc](#)[Printer-friendly Version](#)[Interactive Discussion](#)

## Evaluation of a chemistry transport model using a regional OMI NO<sub>2</sub> retrieval

G. Kuhlmann et al.

Title Page

Abstract

Introduction

Conclusions

References

Tables

Figures

◀

▶

◀

▶

Back

Close

Full Screen / Esc

Printer-friendly Version

Interactive Discussion



**Table 4.** The difference between raw and processed CMAQ data due to the spatial resolution of the satellite instrument (area averaging error).

	IOA	$r$	MB <sup>a</sup>	NMB <sup>b</sup>	RMSE <sup>a</sup>	CV <sup>b</sup>
HK & SZ	0.54	+0.25	−4.6	−16	17.6	59
FS & GZ	0.77	+0.67	−1.6	−12	7.0	52
all stations	0.69	+0.56	−2.9	−17	9.3	54

<sup>a</sup> in ppbv, <sup>b</sup> in percent.



## Evaluation of a chemistry transport model using a regional OMI NO<sub>2</sub> retrieval

G. Kuhlmann et al.

Title Page

Abstract

Introduction

Conclusions

References

Tables

Figures

◀

▶

◀

▶

Back

Close

Full Screen / Esc

Printer-friendly Version

Interactive Discussion



**Table 5.** OMI evaluation with the RAQM network.

Case	IOA	$r$	MB <sup>a</sup>	NMB <sup>b</sup>	RMSE <sup>a</sup>	CV <sup>b</sup>
Hong Kong and Shenzhen						
SP2	0.31	+0.19	-17.5	-54	23.4	73
PRD-1	0.43	+0.24	-8.8	-27	20.6	64
PRD-2	0.52	+0.25	-0.7	-2	21.9	68
PRD-3	0.44	+0.20	-6.3	-20	20.7	64
PRD-4	0.45	+0.24	-7.4	-23	20.1	62
Foshan and Guangzhou						
SP2	0.43	+0.47	-14.3	-48	20.9	71
PRD-1	0.48	+0.41	-10.7	-36	19.2	65
PRD-2	0.58	+0.42	-5.2	-18	17.8	60
PRD-3	0.50	+0.40	-8.5	-29	18.4	62
PRD-4	0.53	+0.46	-8.7	-29	17.9	60
All stations						
SP2	0.40	+0.35	-10.7	-41	18.7	73
PRD-1	0.46	+0.31	-5.6	-22	18.2	71
PRD-2	0.53	+0.32	+0.7	+3	19.6	76
PRD-3	0.47	+0.29	-3.3	-13	18.6	72
PRD-4	0.50	+0.35	-3.9	-15	17.6	68

<sup>a</sup> in ppbv, <sup>b</sup> in percent.

## Evaluation of a chemistry transport model using a regional OMI NO<sub>2</sub> retrieval

G. Kuhlmann et al.

Title Page

Abstract

Introduction

Conclusions

References

Tables

Figures

◀

▶

◀

▶

Back

Close

Full Screen / Esc

Printer-friendly Version

Interactive Discussion

**Table 6.** NO<sub>2</sub> mean values (in ppbv) at the RAQM network stations for CMAQ, network and OMI datasets.

Stations	CMAQ (raw)	CMAQ (processed)	RAQM	SP2	PRD-1	PRD-2	PRD-3	PRD-4
HK & SZ	29.3	25.1	32.9	14.9	23.4	31.6	25.9	24.8
FS & GZ	13.7	12.0	29.5	15.2	18.9	24.4	21.0	20.8
All stations	18.6	15.7	25.3	14.5	19.4	25.6	21.6	21.0

## Evaluation of a chemistry transport model using a regional OMI NO<sub>2</sub> retrieval

G. Kuhlmann et al.

Title Page

Abstract

Introduction

Conclusions

References

Tables

Figures

◀

▶

◀

▶

Back

Close

Full Screen / Esc

Printer-friendly Version

Interactive Discussion



**Table 7.** Evaluation of the time series of CMAQ with OMI NO<sub>2</sub> VCDs in the two areas marked in Fig. 4.

Dataset	OMI Mean <sup>a</sup>	IOA	<i>r</i>	MB <sup>a</sup>	NMB <sup>b</sup>
Foshan and Guangzhou (area)					
SP2	2.5	0.57	0.37	−0.5	−18
PRD-1	3.1	0.55	0.35	−1.1	−35
PRD-2	4.0	0.51	0.35	−2.0	−49
PRD-3	3.5	0.56	0.43	−1.5	−42
PRD-4	3.4	0.54	0.37	−1.3	−40
Hong Kong and Shenzhen (area)					
SP2	1.7	0.51	0.57	+1.2	+73
PRD-1	2.4	0.65	0.51	+0.6	+24
PRD-2	3.2	0.66	0.45	−0.2	−8
PRD-3	2.7	0.75	0.58	+0.2	+9
PRD-4	2.6	0.71	0.56	+0.4	+15

<sup>a</sup> in 10<sup>16</sup> molecules cm<sup>−2</sup>, <sup>b</sup> in percent.

## Evaluation of a chemistry transport model using a regional OMI NO<sub>2</sub> retrieval

G. Kuhlmann et al.

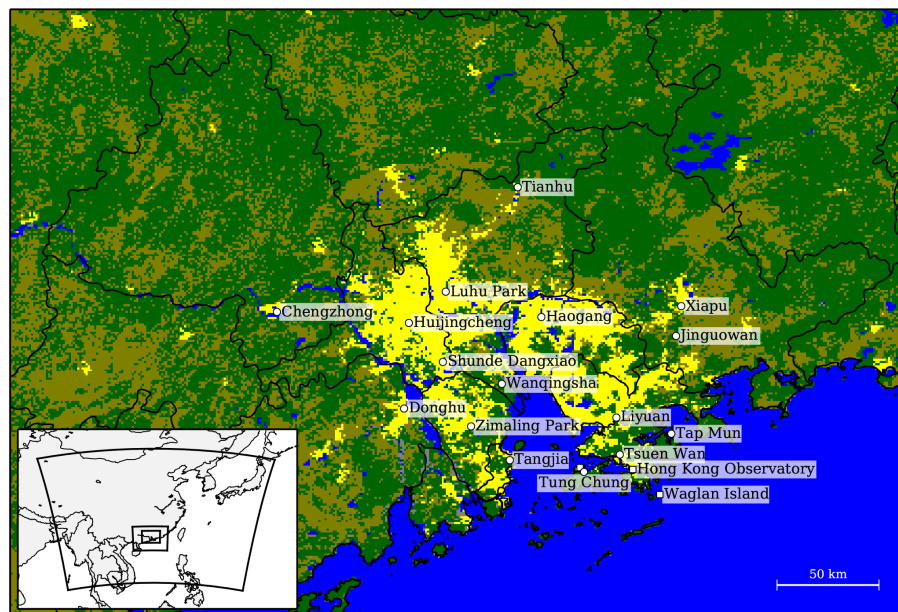


**Figure 1.** The large figure shows the CMAQ model domain (D3) with MODIS land categories in the Pearl River Delta (PRD) region grouped into the following categories: forest (darkgreen), crop lands (olive), bare land (grey), urban areas (yellow) and water (blue). The stations of the PRD Regional Air Quality Monitoring (RAQM) network and HKO automatic weather stations are marked by circles and squares, respectively. The small figure shows the three CMAQ model domains which are D1, D2 and D3 from the largest to smallest.

Title Page

Abstract

Introduction

Conclusions

References

Tables

Figures

◀

▶

◀

▶

Back

Close

Full Screen / Esc

Printer-friendly Version

Interactive Discussion

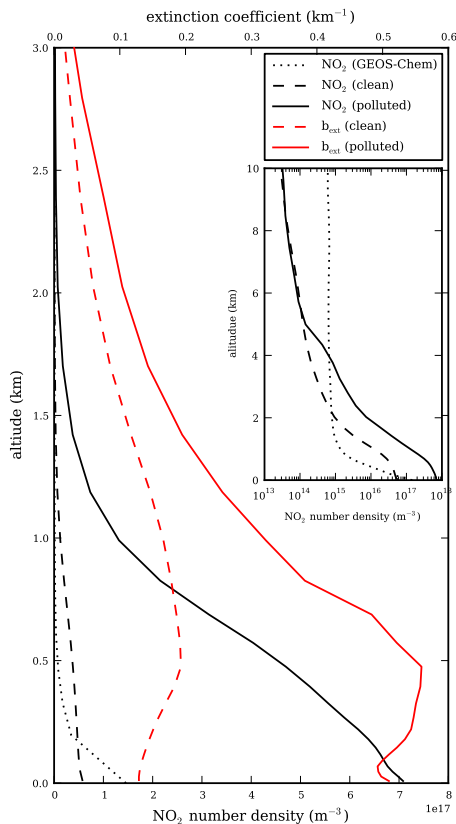


**Figure 2.** Averaged CMAQ  $\text{NO}_2$  and  $b_{\text{ext}}$  profiles under “clean” and “polluted” conditions. A  $\text{NO}_2$  profiles was categorised as polluted, if the ground number density was larger than  $4.8 \times 10^{17} \text{ m}^{-3}$  (about 20 ppbv). A  $b_{\text{ext}}$  profile was categorised as polluted, if the ground extinction coefficient was larger than 0.4. The clean  $b_{\text{ext}}$  profile has an AOT of 0.3 while the polluted as an AOT of 0.6. In addition, an annual GEOS-Chem  $\text{NO}_2$  profile is shown for Hong Kong ( $2^\circ \times 2.5^\circ$  spatial resolution).

## Evaluation of a chemistry transport model using a regional OMI NO<sub>2</sub> retrieval

G. Kuhlmann et al.

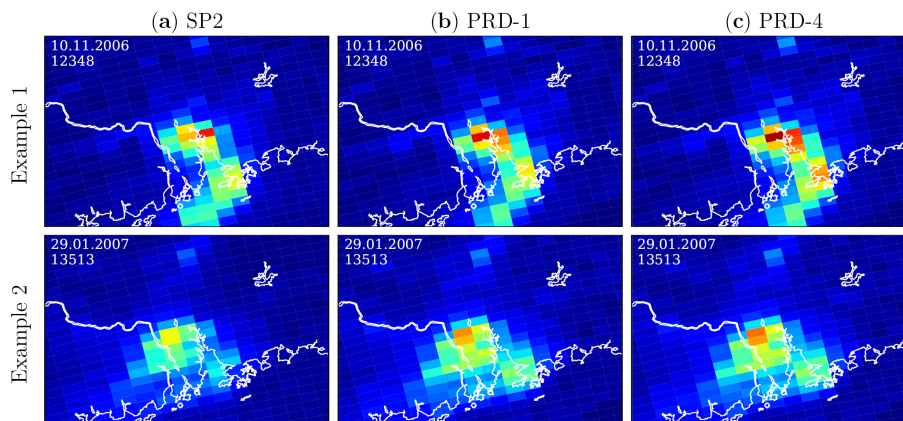


**Figure 3.** Two example orbits of OMI NO<sub>2</sub> distributions for SP2, PRD-1 and PRD-4. The overall spatial distribution is similar but different in details. The PRD-1 and PRD-4 datasets have larger NO<sub>2</sub> column densities than the standard product (SP2).

[Title Page](#)[Abstract](#)[Introduction](#)[Conclusions](#)[References](#)[Tables](#)[Figures](#)[◀](#)[▶](#)[◀](#)[▶](#)[Back](#)[Close](#)[Full Screen / Esc](#)[Printer-friendly Version](#)[Interactive Discussion](#)

## Evaluation of a chemistry transport model using a regional OMI NO<sub>2</sub> retrieval

G. Kuhlmann et al.

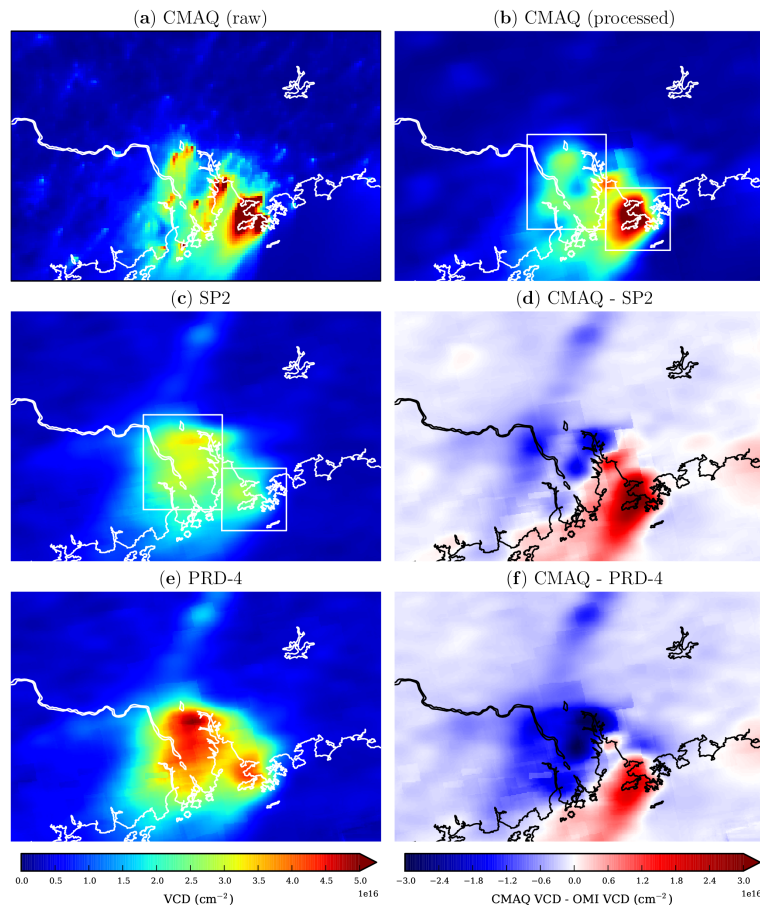


**Figure 4.** Four-month mean distribution of (a) raw and (b) processed CMAQ NO<sub>2</sub> VCDs, (c) OMI SP2 VCDs and (d) the difference to CMAQ, (e) OMI PRD-4 VCDs and (f) the difference to CMAQ.

## Evaluation of a chemistry transport model using a regional OMI NO<sub>2</sub> retrieval

G. Kuhlmann et al.

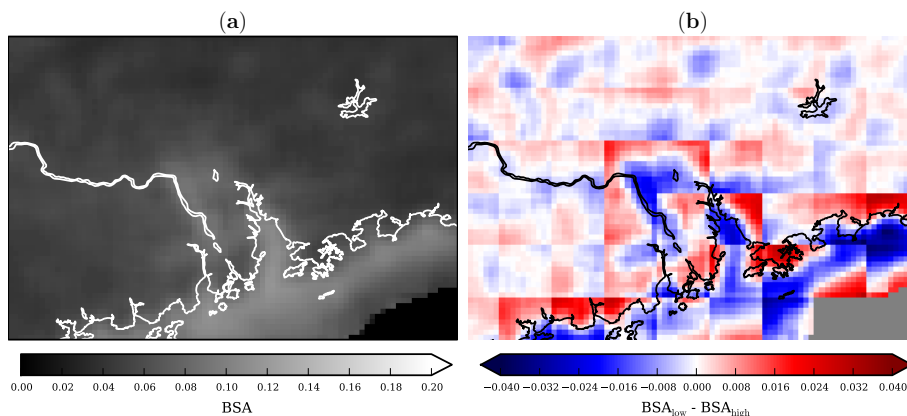


**Figure 5.** (a) The averaged MODIS black-sky albedo (BSA) and (b) the differences between low- and high-resolution BSAs.

Title Page

Abstract

Introduction

Conclusions

References

Tables

Figures

◀

▶

◀

▶

Back

Close

Full Screen / Esc

Printer-friendly Version

Interactive Discussion



## Evaluation of a chemistry transport model using a regional OMI NO<sub>2</sub> retrieval

G. Kuhlmann et al.

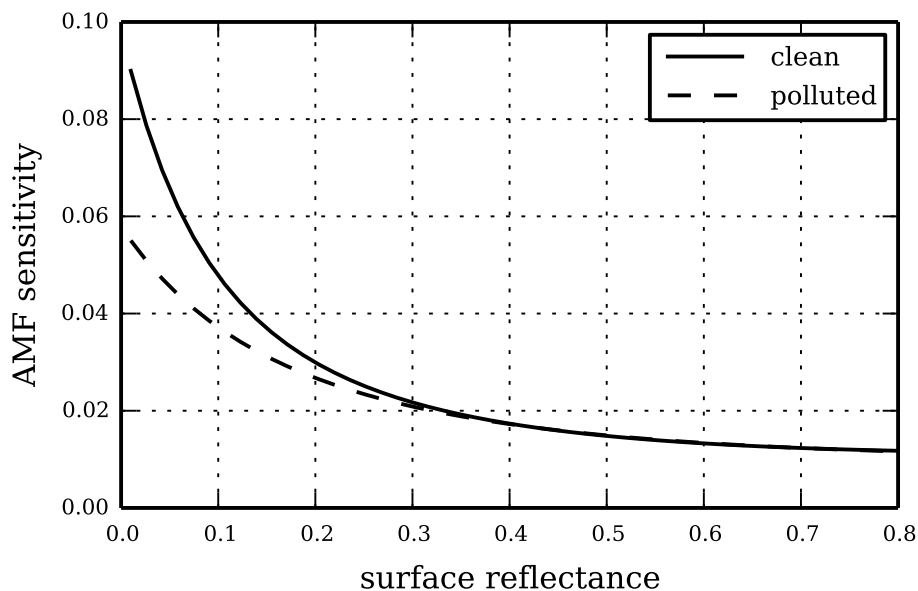


**Figure 6.** Sensitivity of AMF to a change of 0.01 in surface reflectance for different surface reflectance. The lines show the sensitivity for a polluted and clean aerosol profile (Fig. 2).

[Title Page](#)[Abstract](#)[Introduction](#)[Conclusions](#)[References](#)[Tables](#)[Figures](#)[◀](#)[▶](#)[◀](#)[▶](#)[Back](#)[Close](#)[Full Screen / Esc](#)[Printer-friendly Version](#)[Interactive Discussion](#)

## Evaluation of a chemistry transport model using a regional OMI NO<sub>2</sub> retrieval

G. Kuhlmann et al.

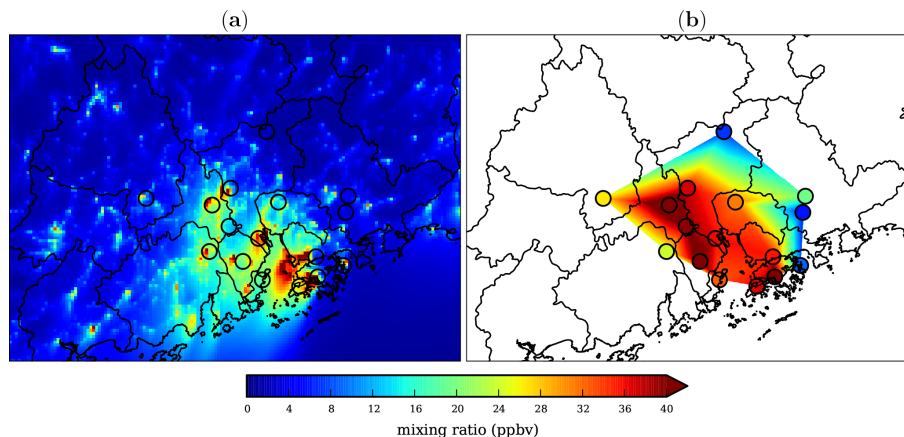


**Figure 7.** Ground level NO<sub>2</sub> mixing ratios averaged for October 2006 to January 2007: **(a)** CMAQ simulation and **(b)** RAQM network measurements. The values between stations have been estimated by linear interpolation.

Title Page

Abstract

Introduction

Conclusions

References

Tables

Figures

◀

▶

◀

▶

Back

Close

Full Screen / Esc

Printer-friendly Version

Interactive Discussion



## Evaluation of a chemistry transport model using a regional OMI $\text{NO}_2$ retrieval

G. Kuhlmann et al.

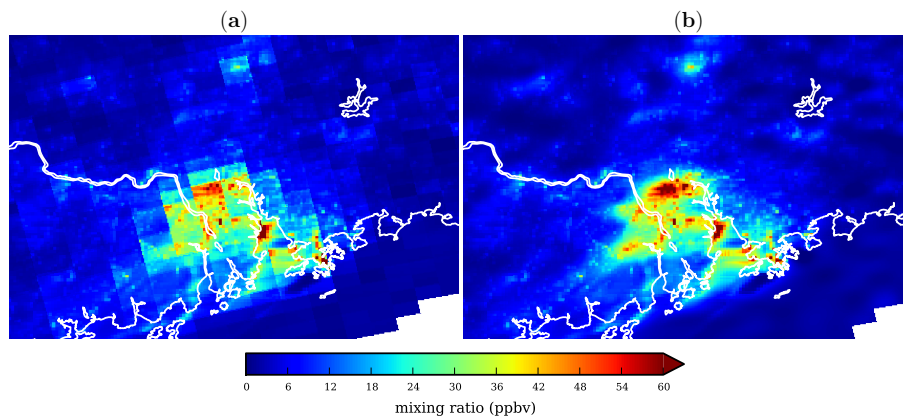


**Figure 8.** OMI ground mixing ratios from orbit number 13513 on 29 January 2007 comparing a **(a)** “standard” and **(b)** newly developed gridding algorithm (Kuhlmann et al., 2014). The discontinuous map created by the “standard” algorithm is difficult to interpret while the new algorithms makes an analysis of the spatial distribution easier.

[Title Page](#)[Abstract](#)[Introduction](#)[Conclusions](#)[References](#)[Tables](#)[Figures](#)[◀](#)[▶](#)[◀](#)[▶](#)[Back](#)[Close](#)[Full Screen / Esc](#)[Printer-friendly Version](#)[Interactive Discussion](#)

## Evaluation of a chemistry transport model using a regional OMI NO<sub>2</sub> retrieval

G. Kuhlmann et al.

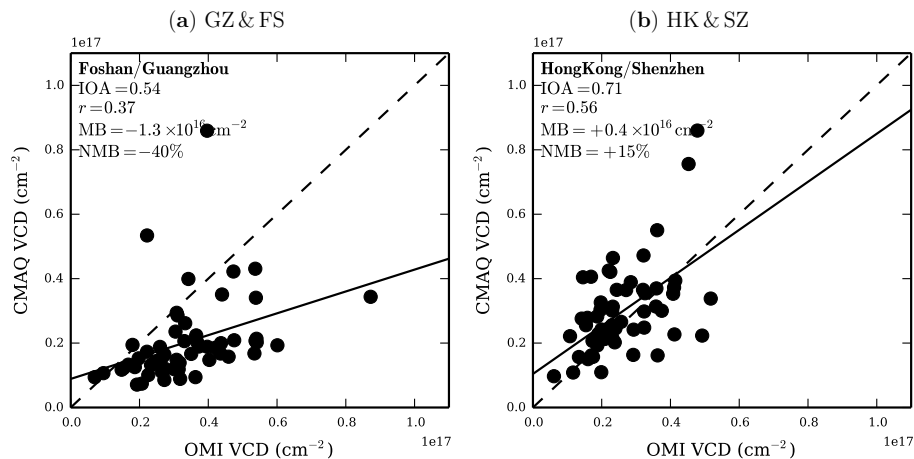


Figure 9. Scatter plot between CMAQ and PRD-4 at (a) GZ & FS and (b) HK & SZ.

[Title Page](#)[Abstract](#)[Introduction](#)[Conclusions](#)[References](#)[Tables](#)[Figures](#)[◀](#)[▶](#)[◀](#)[▶](#)[Back](#)[Close](#)[Full Screen / Esc](#)[Printer-friendly Version](#)[Interactive Discussion](#)